Optical Interaction of Space and Wavelength in High-Resolution Digital Imagers

Brian Rodricks[(a)], Kartik Venkataraman[(a)], Peter Catrysse[(b)] Brian Wandell[(b)]
[a]Micron Technology, Inc., San Jose, CA 95131
[b]Stanford University, Stanford, CA 94305

Precise simulation of digital camera architectures requires an accurate description of how the radiance image is transformed by optics and sampled by the image sensor array. Both for diffraction-limited imaging and for all practical lenses, the width of the optical-point-spread function differs at each wavelength. These differences are relatively small compared to coarse pixel sizes (6μm–8μm). But as pixel size decreases, to say 1.5μm–3μm, wavelength-dependent point-spread functions have a significant impact on the sensor response. We provide a theoretical treatment of how the interaction of spatial and wavelength properties influences the response of high-resolution color imagers. We then describe a model of these factors and an experimental evaluation of the model's computational accuracy.

Keywords: pixel crosstalk; CMOS sensor; spatial resolution; color balancing; color correction

1. INTRODUCTION

Digital image quality depends on the properties of the imager and the image processing algorithms (rendering pipeline) that follow. To obtain high quality images, the algorithms and imager properties must be coordinated. For example, rendering pipeline parameters that govern sharpening, smoothing, de-noising, and color transforms are normally derived from measurements of imager properties; various sensor calibration procedures are available to measure the imager properties. Measurements of sensor noise are important for setting smoothing and sharpening parameters; pixel spectral sensitivity measurements are essential for setting color transformation parameters.

In nearly all current applications, spatial and spectral imager properties are grouped separately and measured in distinct calibration procedures. Similarly, the rendering pipeline separately manages spatial and color transformations. But, as technology scales and pixels become very small, spatial and spectral factors begin to interact so that separate management of space and color can lead to unwanted artifacts. In this paper we describe and quantify one of the factors that confound pattern and color measurements.

The literature describes several types of failures of spatial and spectral independence, and several of these are summarized by the term *pixel crosstalk*. This term refers to pixel responses arising from light incident at neighboring pixels rather than the pixel itself. In a color imager, pixel crosstalk occurs when, say, photons incident on a red pixel produce responses in a neighboring green pixel. Such crosstalk degrades the spatial resolution, reduces overall sensitivity, reduces color separation and increases image noise during color correction procedures.[1]

Pixel crosstalk arises for both optical and electrical reasons. Electrical crosstalk occurs when charge carriers (electrons) generated by incident photons within the nominal pixel-collection region diffuse within the silicon substrate and are collected in a neighboring pixel. The proportion of carriers accumulated by a neighboring pixel depends on the pixel structure, collection area, and distribution of sensitivity inside a pixel. This type of crosstalk even depends on the wavelength of the incident light. This effect occurs because carriers at different depths in the substrate have different likelihoods of reaching neighboring regions, and photons at different wavelengths are likely to be absorbed at different depths. Electrical crosstalk has been studied extensively.[2,3]

Optical crosstalk also has a spectral and a spatial component.[1,4,5] One source of optical crosstalk can be traced to the fact that color filters are located at a considerable distance from the pixel substrate. In modern sensors, the distance from the color filter to the photodetector can be 3μm –7μm, much larger than the photodetector or pixel width. The path from the color filter to the detector contains metal and insulation layers, and each surface boundary scatters some of the incident light. Consequently, light incident at oblique angles can pass through the filter of a particular pixel and

Digital Photography II, edited by Nitin Sampat, Jeffrey M. DiCarlo, Russel A. Martin,
Proc. of SPIE-IS&T Electronic Imaging, SPIE Vol. 6069, 606904, © 2006 SPIE-IS&T · 0277-786X/06/$15

be partially absorbed by the detector in an adjacent pixel. The fraction of light absorbed by a neighboring pixel can vary significantly, and for imaging lenses with a low f-number this scattering can be quite large. Appropriately positioned microlenses located on the top of color filters can significantly reduce spatial optical crosstalk.[1]

However, this is not the only source of optical crosstalk: Wavelength-dependent point-spread functions of the imaging lens provide a different mechanism of optical crosstalk generation.[6, 7] Differences in the light spread as a function of wavelength have a significant impact on the spectral response of pixels near an edge, line, or other fine image feature. The wavelength-dependent spreading of light near an edge or line means that the spectral power distribution of the light incident at a pixel depends on the pixel's position with respect to that edge or line. Furthermore, the spectral power distribution of light falling on pixels near an edge varies with position, even when the spectral power distribution in the scene is constant across space. Hence, color measurements made by pixels near an edge or line are unreliable measures of scene color.

The precise spectral composition of the light near an edge depends on the spatial structure in the image. This interaction of pattern and color produces a highly complex relationship between the spectral illumination at the pixel and the scene pattern. Accounting for these complex local effects is probably beyond the level of complexity of current rendering pipeline technologies. On the other hand, it is best to avoid using the color responses near edges to infer color properties about the scene, such as the color of the illumination.

In addition to local spatial-spectral interactions, further interactions between spatial and spectral variables can be traced to variations in the on- and off-axis point-spread functions. Because the point spread changes slowly across space, the trend associated with this effect also changes slowly across the field of view. Hence, it may be possible to detect and correct this effect in conventional imagers.

The interaction between wavelength and spatial spreading results in a photodetector signal that is similar to other pixel crosstalk effects, because wavelength-dependent point-spread functions have a particularly powerful effect on imagers with small pixels (less than 2μm). We provide a theoretical treatment of this phenomenon, and we illustrate its effects through simulation.

2. METHODS

We use the Image Systems Evaluation Tools (ISET) software to analyze how the interaction of spatial and wavelength properties influences the response of high resolution color imagers.[8] This software models the imaging pipeline by specifying (1) a radiometric description of the scene, (2) optical transformation of the scene radiance to the irradiance signals at the sensor, (3) sensor capture, (4) digital image processing for display, and (5) several perceptual metrics. In this section, we describe the analytical formula used in the simulation with a particular emphasis on the image formation methods.

ISET simulations can be initiated from a scene model; this is a radiometric dataset in which each pixel represents the spectral radiance $L(x, y; \lambda)$ at a spatial location in a plane at a fixed distance (x, y). The radiance is expressed in units of $W/(s\,m^2\,sr\,nm)$, which can be converted to photons. The imaging optics convert the scene spectral radiance to a spectral irradiance image incident on the image sensor, $E(x, y; \lambda)$ in $W/(s\,m^2\,nm)$. When modeling diffraction-limited optics, the ideal geometric image irradiance distribution is calculated by the camera equation,[9]

$$E(x, y; \lambda) = \frac{\pi T(\lambda) R(x, y; \lambda)}{1 + 4(1-m)^2 (f/\#)^2} L\left(\frac{x}{m}, \frac{y}{m}; \lambda\right), \quad (1)$$

where $T(\lambda)$ is the lens spectral transmittance, $R(x, y; \lambda)$ is a relative illumination factor that accounts for off-axis irradiance, and m (< 0) is the magnification. The term

$$f/\# = \frac{f}{D} \tag{2}$$

is the f-number of the imaging system, a dimensionless quantity equal to the ratio of the lens focal length and the diameter of the clear aperture.

ISET includes a variety of imaging optics models, ranging from an ideal diffraction-limited lens to realistic lens models that include all the effects of monochromatic and chromatic aberrations, pupil aberrations, vignetting, and diffraction.[7] Of particular relevance to the calculations here, the blurring process is characterized by a wavelength-dependent convolution operation,[10]

$$E_{image}(x,y;\lambda) = PSF(x,y;\lambda) \otimes E(x,y;\lambda), \tag{3}$$

where $PSF(x,y;\lambda)$ is the point-spread function of the imaging lens and $\otimes$ denotes the convolution operator. This convolution operation is valid over small image regions (isoplanatic). In the most general calculation, the image plane is divided into small isoplanatic sections, and each section is associated with a point-spread function.[7] Each point-spread function has unit area under the curve, ensuring that no photons are lost by the blurring process. For a diffraction-limited system, the optical transfer function (OTF), which is the two-dimensional Fourier transform of the PSF, is[10]

$$OTF(\rho;\lambda) = \begin{cases} \frac{2}{\pi}\left[\arccos\left(\frac{\rho}{2\rho_0}\right) - \frac{\rho}{2\rho_0}\sqrt{1-\left(\frac{\rho}{2\rho_0}\right)^2}\right] & \rho \le 2\rho_0 \\ 0 & otherwise \end{cases}, \tag{4}$$

where $\rho = \sqrt{f_x^2 + f_y^2}$ is the general radial distance in the spatial frequency plane and $\rho_0 = 1/(2\lambda f/\#)$. Because the PSF has unit-area at each wavelength, $OTF(0;\lambda) = 1$. The peak of a unit-area point-spread function, located at (0,0), can be derived from the area under the normalized OTF

$$PSF(0,0;\lambda) = \int_{-\infty}^{\infty}\int_{-\infty}^{\infty} OTF(f_x, f_y;\lambda)\, df_x df_y = \frac{\pi}{4}\frac{1}{\lambda^2 f/\#^2}. \tag{5}$$

Equation 7 shows that the peak of the PSF varies (inversely) with the square of the wavelength.

The line-spread function (LSF) is the inverse one-dimensional Fourier Transform of the radial OTF

$$LSF(r;\lambda) = \int_{-\infty}^{\infty} OTF(\rho;\lambda) e^{j2\pi\rho r}\, d\rho. \tag{6}$$

The peak of the LSF can be derived from the area under the radial OTF as well,

$$LSF(0;\lambda) = \int_{0}^{2\rho_0} OTF(\rho;\lambda)\, d\rho = \frac{4}{3\pi}\frac{1}{\lambda f/\#}. \tag{7}$$

Equation 9 shows that the peak of the LSF varies (inversely) with wavelength.

The remainder of the optical path, from sensor surface to silicon substrate, includes: a microlens, a color filter, planarization and interconnect layers, contacts, vias and dielectric layers that wire active devices into circuits. Different

approaches can be taken to characterize this part of the optical path; we analyze the behavior of on- and off-axis pixels using a phase-space approach.[11] The relationship between the surface irradiance image and the image incident on the silicon substrate can be summarized by an optical efficiency,[11]

$$E_{substrate}(x,y;\lambda) = OE(x,y;\lambda)\,E_{image}(x,y;\lambda). \tag{8}$$

For color image sensors, each color channel has its own optical efficiency: OE_R, OE_G, and OE_B. These optical efficiencies include the appropriate color-filter transmission properties.

An electrical path follows the optical path, and converts of the optical image into a voltage image,

$$V(x,y) = gAt_{\exp}\int QE(\lambda)\,E_{substrate}(x,y;\lambda)\frac{hc}{\lambda}d\lambda, \tag{9}$$

where g is the conversion gain in $\mu V/e^-$, A is the photodetector area inside the pixel in m^2, $t_{\exp}$ is the exposure time in s, $QE(\lambda)$ is the spectral quantum efficiency, which describes the conversion efficiency from photons to electrons, c is the speed of light in vacuum, and h is Planck's constant. The voltage image is digitized to form a digital representation of the captured image. The ISET software includes a quantitative model of the photodetector that accounts for a variety of sensor parameters, such as pixel fill-factor, dark noise, read noise, and many others. The software also includes a variety of image processing algorithms, such as demosaicing, color conversion, and color balancing, and rendering methods; for example, to allow the digital image to be viewed on a monitor. In addition, it includes metrics to evaluate the perceptual quality of the final rendered image.[8] The software implementation of these calculations and scripts to generate the figures for this paper are available at www.imageval.com.

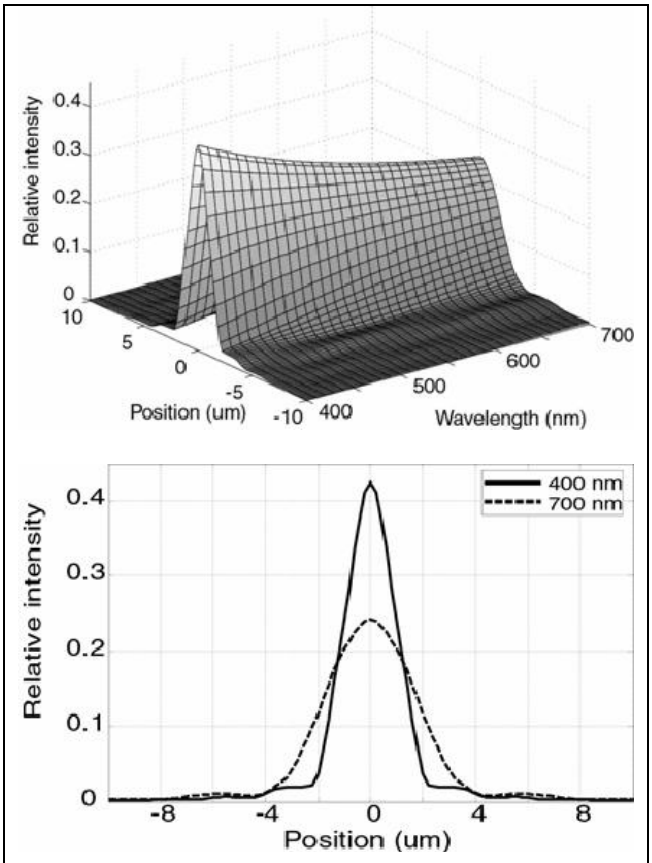

Figure 1. Wavelength-dependent spatial blurring of a diffraction-limited f/5.6 lens. The surface (top) represents line spread functions from 400nm–700nm. The graph (bottom) compares the functions at 400nm and 700 nm directly.

3. RESULTS

The main results of this paper show how scene spatial and spectral properties interact to form the spectral irradiance image at the sensor surface. The spatial-spectral interactions we analyze arise from the wavelength-dependent properties of the point-spread function (PSF). The first results illustrate the spatial-spectral interaction at the level of the irradiance image, using simple patterns and diffraction-limited optics. The second measure shows the significance of these interactions for the sensor response as pixel size varies. The third results show how the spatial-spectral interactions vary between on-axis and off-axis image sections using an example lens.

Diffraction-limited spatial-spectral interactions. The wavelength-dependent spatial blurring of a diffraction-limited f/5.6 lens is illustrated in Figure 1a. The surface represents the line spread function at different wavelengths. The spatial spread of the line spread function increases from 400nm to 700nm. This

wavelength-dependent spreading has two consequences. First, the peak of the line spread decreases as wavelength increases. Hence, spatial blurring decreases the number of photons at the center of the line image; this is captured by the declining peak amplitude, which is much higher at 400nm than 700nm. The reverse phenomenon is present a short distance (2µm–4µm) from the peak. The long-wavelength photons are spread farther from the line center. Hence, more long- than short-wavelength photons are present 3µm from the peak. The wavelength-dependent blurring causes pixels at different positions to experience different spectral irradiance functions. None of these functions matches the spectral photon radiance of the original image, which is constant across wavelength.

The difference in spatial blurring between 400nm and 700nm light is illustrated in Figure 1b, where the line spread functions at 400nm and 700nm are directly compared. The full-width half-maximum (FWHM) of the 400nm line spread is roughly 2µm, while the FWHM for the 700nm line is roughly 4µm. For this diffraction-limited f/5.6 lens, a pixel covered by a filter that transmits only short-wavelength light (blue) will be exposed to an image that has significantly better spatial resolution than a pixel that responds only to long-wavelength light.

The plotted curves also show that the spectral photon distribution (SPD) of the light in the irradiance depends upon the spatial pattern in the scene image. At the center of the line's image, the SPD declines with wavelength, even though the input scene has a uniform SPD. The spectral irradiance at the peak is specific to this lens, but the basic phenomenon is present for any diffraction-limited lens. The SPD change can become very large when the image contains many lines or edges. Figure 2 illustrates the effect using a scene pattern with many lines. The scene is composed of a set of grid lines; each line is modeled as having a constant spectral photon distribution (SPD; see Figure 2 inset, upper left). The main image represents the spectral irradiance at the imager after accounting for the properties of the f/5.6 diffraction-limited optics.

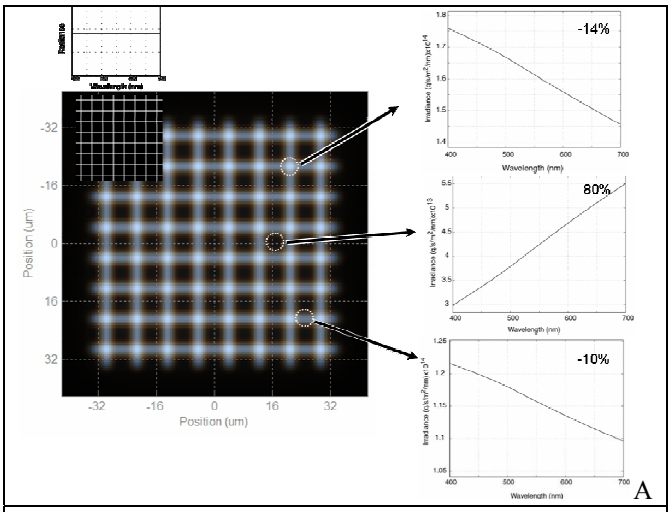

Figure 2. The simulated irradiance image of a scene of grid lines (f/5.6, diffraction-limited); the scene is shown in the inset at the upper left. Lines have a uniform spectral photon density (SPD); the main image represents the optical image on a spatial scale; and curves at the right show the large variation in the SPD by comparing three regions: near the line intersection (top), the holes (middle), or along a line (bottom).

The image is superimposed on a spatial grid to make it easy to compare the spreading with typical pixel sizes. The pointspread causes the grid lines to spread across several microns, covering distances that exceed 2µm, a typical small pixel size. Furthermore, the irradiance SPD varies at these different locations. The SPD near grid line intersections is similar to that of the line spread function's peak, with a higher representation of short- rather than long-wavelength light. The SPDs measured in the dark regions between the fine grid lines have relatively more long-wavelength photons. These are contributed by the spreading of long-wavelength photons from all of the intersections surrounding the hole. Note that the SPD in the dark regions is still at a fairly high intensity level, being only about one order of magnitude lower than the levels at the intersections.

Consequently, even though the scene image contains only a single uniform SPD, the SPD in the irradiance varies significantly across space, and neighboring pixels are exposed to very different SPDs. It follows that, in image regions containing fine patterns, the spectral irradiance image is an unreliable measure of the scene SPD. It would be unwise, for example, to use the measurements from individual pixels in such regions to estimate scene SPD, because the irradiance SPD depends very strongly on the spatial structure of the image.

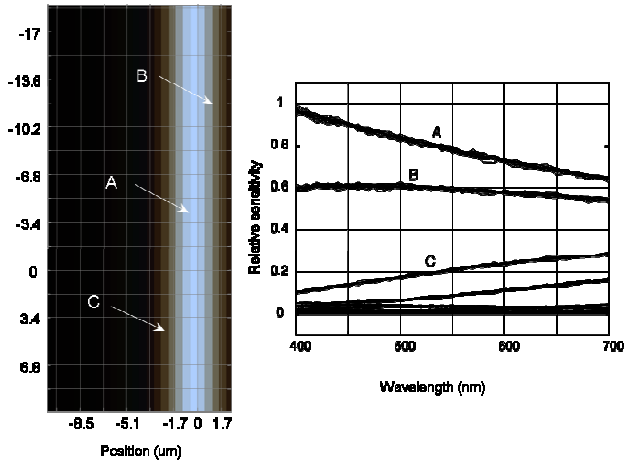

Figure 3. Pixel spectral response curves measured using a line stimulus with a constant (flat) spectral photon distribution (SPD). Because of the wavelength-dependent spreading, irradiance at the imager becomes uneven. Hence, the irradiance image at different locations does not match the equal photon input, and pixels at various distances from the center of the line appear to have different spectral response properties.

It is possible to compensate for spatial non-homogeneity in the irradiance SPD by pooling information across pixels; the average SPD of the irradiance image matches the SPD of the scene. But choosing the "right" region to average is not practical in a complex image. On the whole, it seems that only the spectral irradiance information in relatively uniform (coarse) image regions should be used to safely estimate the scene SPD. The specific meaning of "coarse" will depend on the quality of the optics. For the diffraction-limited f/5.6 lens used in this simulation, the SPD of an in-focus image region varies strongly over a range of 6μm–8μm. For these optics, which would be ideal optics for a structure with the human pupil and focal length, the irradiance should be approximately constant over a spatial extent of more than three times that distance (30μm; scene visual angle of 0.1 degree) to have a constant central region whose SPD matches that of the scene. This size is much coarser than the resolution limit of the human eye, which is on the order of 0.017 degrees of visual angle.[12]

Next, we simulate an experimental measurement of pixel spectral quantum efficiency. This simulation verifies the calculations and illustrates the size of the effects of the changing SPD on an image sensor response. First, we simulate a set of sensor measurements obtained with a spatially uniform field of light at a series of different wavelengths. The sensor pixels are 2μm (100 percent fill-factor) and modeled as having a constant spectral QE. The number of photons within each waveband is equal, and we use the simulated voltage response as an estimate of the relative spectral QE.

When the simulation is performed using a spatially uniform field, we recover the uniform spectral quantum efficiency as expected (not shown). But, the same simulation is performed using a thin line rather than a uniform spatial field, the estimated spectral QE varies strongly across pixel position, shown in Figure 3. The variation occurs because image formation redistributes the image photons according to their wavelength; photons at different wavelengths are distributed by different amounts in the irradiance image. Short-wavelength photons remain mainly near the center of the line (position A). But long-wavelength photons are spread and fall in disproportionately large quantities at the margins of the line (position C). Intermediate positions have intermediate spectral QE estimates (position B). The relative intensity at the center is much higher than the intensity at the margin, but the difference in the mean response is only a factor of four; responses from the margin are still significant. The simulation shows that measured voltage responses depend on the wavelength of light in the line, but the spectral QE varies by pixel position. Importantly, the estimated spectral QEs do not reflect the true pixel spectral QE, which is constant across wavelength.

There are at least two cases in which these interactions limit color imaging. First, the basic assumptions of spatial demosaicing—that the image has a single spectral irradiance across the 2x2 array—are strongly violated near edges. In modern imagers with 2μm pixels, there will be a spatial variation across the 2x2 pattern of a Bayer color filter array and the 4μm period of the Bayer color filter array pattern will often produce inaccurate renderings unless care is taken to handle the edges in a special way. Second, the irradiance SPD at these pixels does not match the scene SPD. Hence, the color responses from pixels near an edge do not measure to scene SPD. These responses should probably be excluded in white-point estimation algorithms, or at least accounted for in a systematic way.

Pixel size. These spatial-spectral interactions occur prior to image capture. The impact of these optical factors on sensor response depends on the relationship between pixel size and wavelength-dependent spreading in the image formation process. In general, the impact of spatial-spectral interactions on imager response is of greater magnitude for small than

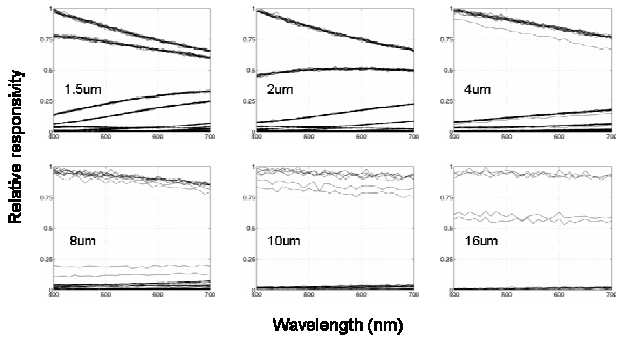

Figure 4. Estimated spectral responsivity of pixels in a monochrome sensor as a function of pixel size. The test stimulus was a line with constant SPD, and a diffraction-limited f/5.6 lens. The pixel sizes were 2µm, 4µm, 8µm, 10µm, and 16µm. For pixel sizes of 2 µm and 4µm, individual pixels experience different spectral irradiance functions depending on the pixel's location relative to the center of the line. The effect's significance declines with pixel size, so that in this example, with the line centered over the pixel, an 8µm or larger pixel experiences only a 5–6 percent effect over a 100nm waveband.

large pixels. The relationship between the size of the effect and pixel size is measured for several simulated sensors in Figure 4. The graphs are estimated pixel spectral QE using sensors with pixels ranging in size from 1.5µm–16µm.

Pixel sizes ranging from 1.5µm–4µm and centered on the line respond more powerfully to short than long-wavelength light. The relative sensitivity increase for 1.5µm–4µm pixels is on the order of 10–20 percent. Pixels at the edge of the line experience different spectral-irradiance functions, and these show a complementary sensitivity increase to long-wavelength photons. As pixel size grows, in the range from 8µm–16µm, the estimated spectral QE becomes increasingly constant. Even though there is a slight bias, it is not very large. For example, a color pixel that measures light within a 100nm waveband sees relatively minor effects at 8µm–16µm or larger. . Also, the responses at the pixels in the center of the line, with the large responses, are similar to the responses of the pixels at the edge of the line.

The reduction of the spectral QE variation with pixel size can be understood from simple properties. When the line image is centered on a large pixel, the response integrates all of the light even though it is spread by the optics. Because of this summation, the pixel response measures the scene SPD. On the other hand, when pixel size is small compared to spread, each pixel responds to a narrow portion of the spread. Spectral response then depends on the pixel's position with respect to wavelength-dependent spreading.

The simulations in Figure 4 illustrate how the spatial-spectral interactions change the spectral QE for one particular pattern in one position. Changing the line position or changing the pattern changes the responses. These effects can be illustrated by simulation, but we have no simple analytical relationships to express the relationship between pattern, optics and imager.

On- and off-axis imaging. To this point, simulations have treated the optics as a single, shift-invariant system (isoplanatic). Real lenses are locally isoplanatic, but their point-spread functions vary with field height. A typical lens is designed to be optimized for on-axis imaging with minimal spatial spreading and wavelength variation in the central portion of the visual field. At increasing field heights, the point-spread function broadens and differences in the point-spread function at the various wavelengths increase. Consequently, the spatial-spectral interactions will differ from the center and periphery of the image. This section of results illustrates the difference between on- and off-axis imaging for an example lens.

Using lens simulation software from Zemax®[13] and a lens prescription for a 2mm aspheric achromatic f/5.6 lens, we created an array of point-spread functions for different wavelengths and field heights.[7] The point-spread functions for an on-axis and a 1.0mm off-axis location are shown in the plots in the left portion of Figure 5 (550nm). The on-axis point-spread function is symmetrical and similar to that of a diffraction limited lens with an f/5.6. The off-axis point-spread function is asymmetrical with an orientation toward the image center. This 'lumpy' point-spread function is due to aberrations (such as a coma) and quite common for off-axis point spreads in real lenses.[14]

In the on-axis simulation (Figure 5 top graphs), the results parallel those in the diffraction-limited case. For this real lens, the short-wavelength photons are scattered less than long-wavelength photons (not shown). Consequently, the estimated spectral QE of the pixels near the center of the line is higher in the short- than long-wavelength portion of the

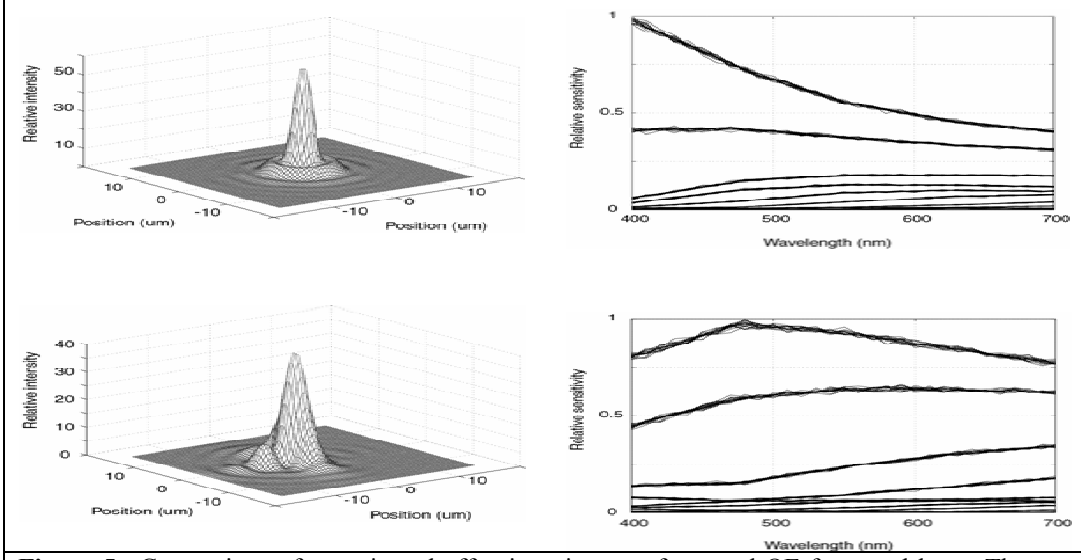

Figure 5. Comparison of on-axis and off-axis estimates of spectral QE for a real lens. The upper panels show the point spread function on-axis and at 1.0mm field height for a 2mm aspheric achromatic f/5.6 lens. These were derived from Zemax® calculations using the lens prescription. The estimated spectral QE of pixels near an equal SPD line are shown in the two bottom panels. The spectral QE differs between the on-axis and off-axis image portions of the image, despite the fact that the scene input and sensor properties are identical across these two regions. The differences introduced by lens imperfections are particularly strong for small pixels (2μm in this case) and can require special space-varying correction.

spectrum. The pixels at the margin of the line image have lower overall sensitivity and their peak spectral QE is in the long-wavelength portion of the spectrum.

The point-spread functions at 1.0mm field height differ from the on-axis functions. The 400nm light is spread more than the 500nm light. This difference is reflected in the estimated spectral QE measured at this field height, shown in the bottom portion of Figure 5. The peak spectral QE for a pixel in the middle of the line's irradiance image is no longer at 400nm, but closer to 500nm. Experimental measurements of the PSFs as a function of wavelength and its spatial variance correlate well with experimental measurements taken on a nearly diffraction limited lens.[15]

The spectral QE trend reverses at the line image's margin, because this location contains the distributed photons. Again, the spectral QE of pixels at the line margin complement the spectral QE of the line center. The relationship between estimated spectral QE and the data is more complex, of course, when the spatial pattern is more complex. But a simple and general point from this analysis is this: spatial-spectral interactions in the on- and off-axis portions of the image differ. The differences introduced by this image formation process can appear as differences in the effective spectral QE of on- and off-axis pixels.

4. DISCUSSION

The spatial-spectral interactions explored in these calculations and simulations are part of the normal image formation process. The effects they produce on pixel response are similar to other, related phenomena known as pixel crosstalk.

Figure 6 illustrates the effect of this spatial-spectral interaction for a color sensor. In this simulation, we modeled a 2μm pixel within a Bayer RGGB pattern. The data in the image are rendered using only bilinear demosaicing. The figure

shows two regions of the image (64x64 pixels); the region on the left is produced by using the on-axis point-spread functions of the 2mm aspheric lens, and the region on the right is modeled using the off-axis (1.0mm field height) point-spread functions.

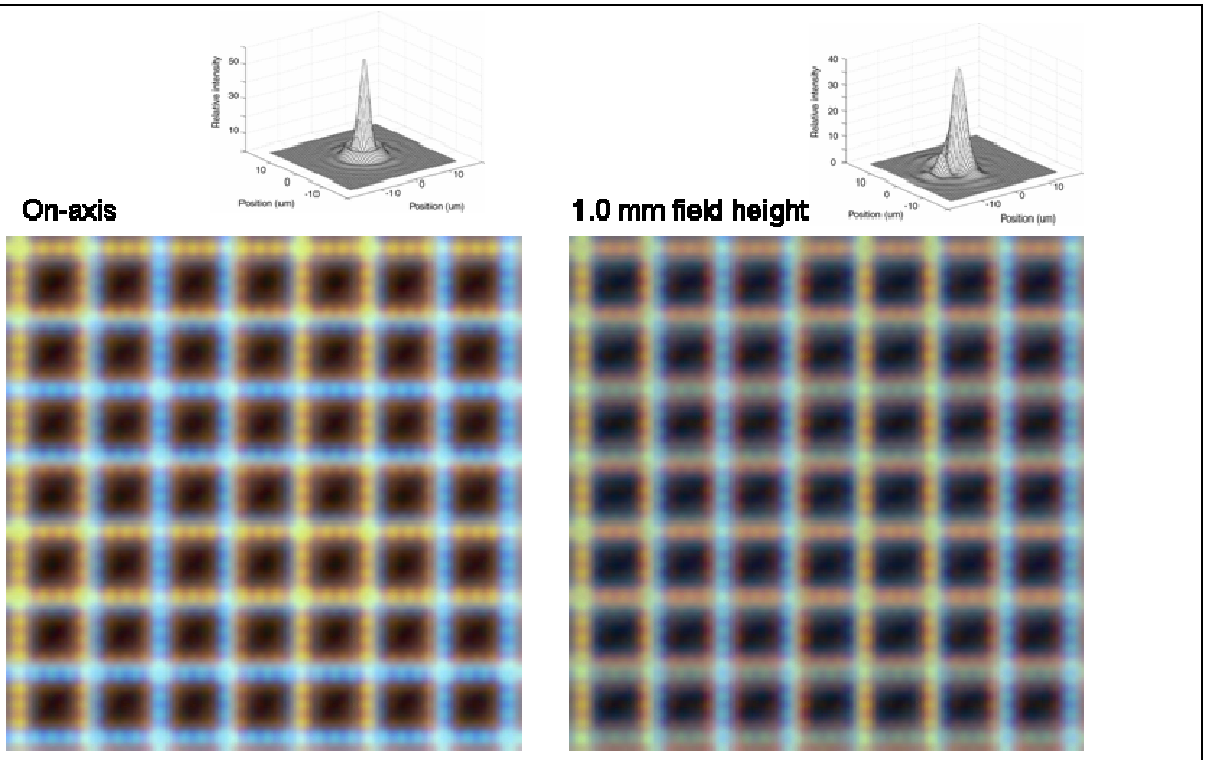

Figure 6. Detail of simulated grid line images for the on-axis and off-axis portions of a color sensor. All scene and sensor properties are identical; only the local point spread functions differ as in Figure 5. With a 2μm pixel, these point-spread function differences cause the renderings to differ significantly.

Color renderings within these two regions differ significantly. Note that the input, sensor properties, and rendering algorithms are identical: the only difference is the model of the local point-spread functions. It is widely understood that differences between on-axis and off-axis image formation produce geometrical distortions and general loss of resolution. The results here show that these differences also produce color shifts that may contribute to the general group of effects known as pixel crosstalk.

As pixels get smaller in size, the wavelength dependence and the field height dependence of the PSFs can produce objectionable artifacts in the image. Much of the image processing now applied, may need to be done on a channel basis. PSF-based focus recovery, spatially dependent cross-talk correction, geometric distortion, and color correction may need to be applied on a channel-wise basis.

ACKNOWLEDGMENTS

The authors thank the team at ImagEval, and particularly Dr. J. E. Farrell, for useful discussions. Peter.Catrysse. acknowledges partial support from a Center for Integrated Systems Fellow/Mentor/Advisor (CIS FMA) fellowship from Agilent Technologies, Inc. Thanks to Dmitry Bakin for help with the PSF measurements and to Pravin Rao for help with the PSF modeling in ISET. Special thanks to Robert Mullis for useful discussions.

REFERENCES

[1] G. Agranov, V. Berezin, and R. H. Tsai, "Crosstalk and microlens study in a color CMOS image sensor," IEEE Trans. Electron Devices **50** (1), 4-11 (2003).

[2] I. Shcherback and O. Yadid-Pecht, "CMOS APS MTF modeling," IEEE Trans. Electron Devices **48** (12), 2710-2715 (2001).

[3] J. S. Lee and R. I. Hornsey, "Photoresponse of photodiode arrays for solid-state image sensors," J. Vac. Sci. Technol., A **18** (2), 621-625 (2000).

[4] Cecile Marques and Pierre Magnan, in *Sensors and Camera Systems for Scientific, Industrial, and Digital Photography Applications III*, edited by Morley M. Blouke, John Canosa, and Nitin Sampat (SPIE, San Jose, CA, USA, 2002), Vol. 4669, pp. 107-116.

[5] D. Ramey and J. Boyd, "Computer simulation of optical crosstalk in linear imaging arrays," IEEE J. Quantum Electron. **17** (4), 553-556 (1981).

[6] Peter B. Catrysse and Brian A. Wandell, in *Digital Photography*, edited by Nitin Sampat, Jeffrey M. DiCarlo, and Ricardo J. Motta (SPIE, San Jose, CA, USA, 2005), Vol. 5678, pp. 1-13.

[7] Patrick Y. Maeda, Peter B. Catrysse, and Brian A. Wandell, in *Digital Photography*, edited by Nitin Sampat, Jeffrey M. DiCarlo, and Ricardo J. Motta (SPIE, San Jose, CA, USA, 2005), Vol. 5678, pp. 48-58.

[8] Joyce E. Farrell, Feng Xiao, Peter B. Catrysse et al., in *Image Quality and System Performance*, edited by Yoichi Miyake and D. Rene Rasmussen (SPIE, San Jose, 2003), Vol. 5294, pp. 124-131.

[9] Miles V. Klein and Thomas E. Furtak, *Optics*, 2nd ed. (Wiley, New York, 1986).

[10] Joseph W. Goodman, *Introduction to Fourier optics*, 2nd ed. (McGraw-Hill, New York, 1996).

[11] P.B. Catrysse and B.A. Wandell, "The optical efficiency of image sensor pixels," J. Opt. Soc. Am. A **19** (8), 1610-1620 (2002).

[12] Brian A. Wandell, *Foundations of vision*. (Sinauer Associates, Sunderland, Mass., 1995).

[13] Zemax (Zemax Development Corporation, 2006).

[14] Warren J. Smith, *Modern optical engineering: the design of optical systems*, 2nd ed. (McGraw-Hill, New York, 1990).

[15] To be published.